Research in Astronomy and Astrophysics, 23:065002 (16pp), 2023 June https://doi.org/10.1088/1674-4527/acca01

Research Progress on Solar Flare Forecast Methods Based on Data-driven Models

Ke Han[1], Meng-Yao Yu[1,2], Jun-Feng Fu[2], Wen-Bin Ling[2], De-quan Zheng[1], Jie Wan[2], and Peng E[2]
[1] School of Computer and Information Engineering, Heilongjiang Provincial Key Laboratory of Electronic Commerce and Information Processing, Harbin University of Commerce, Harbin 150028, China
[2] Laboratory for Space Environment and Physical Sciences, Harbin Institute of Technology, Harbin 150001, China; wanjie@hit.edu.cn
Received 2023 January 8; revised 2023 February 23; accepted 2023 March 6; published 2023 May 10

Abstract

Eruption of solar flares is a complex nonlinear process, and the rays and high-energy particles generated by such an eruption are detrimental to the reliability of space-based or ground-based systems. So far, there are not reliable physical models to accurately account for the flare outburst mechanism, but a lot of data-driven models have been built to study a solar flare and forecast it. In the paper, the status of solar-flare forecasting is reviewed, with emphasis on the machine learning methods and data-processing techniques used in the models. At first, the essential forecast factors strongly relevant to solar flare outbursts, such as classification information of the sunspots and evolution pattern of the magnetic field, are reviewed and analyzed. Subsequently, methods of resampling for data preprocessing are introduced to solve the problems of class imbalance in the solar flare samples. Afterwards, typical model structures adopted for flare forecasting are reviewed from the aspects of the single and fusion models, and the forecast performances of the different models are analyzed. Finally, we herein summarize the current research on solar flare forecasting and outline its development trends.

Key words: Sun: activity – Sun: flares – (Sun:) sunspots – Sun: magnetic fields

1. Introduction

A solar flare, discovered by Carrington (1859) in 1859, is an explosive phenomenon that occurs in the magnetized plasma of the solar atmosphere. The important mechanism governing the flare eruption is considered to be magnetic reconnection (Inoue et al. 2017), which can last from a few minutes to more than ten minutes. In this short period, flares can release massive energy up to 10^{28}–10^{32} J (Shibata & Magara 2011), accompanied by a sudden enhancement in particle radiation.

High-energy particles produced by the solar flare can penetrate the human body and cause biochemical damage. Simultaneously, intensive ultraviolet radiation and X-rays can cause a dramatic increase in the concentration of electrons in the ionosphere, triggering a sudden disturbance of the ionosphere. In addition, they have a significant impact on spacecraft communication, broadcast signals, and satellite navigation. Therefore, to understand the mechanism of solar activity and guarantee the safety of human space exploration, conducting solar flare forecasting, which is of great scientific significance and practical value, is necessary.

In recent years, with the popularization of machine learning (ML) algorithms, flare forecasting methods have evolved from traditional empirical statistical methods to data-driven model-based forecasting methods. The data-driven model-based methods are composed of three steps as follows.

The first step is to select forecast factors. Now, available forecast factors generally describe the non-potentiality and complexity of the solar active regions, which are believed to be strongly related to flare outbursts. Among them, the prevalent two factors are classification information of the sunspots and evolution pattern of the magnetic field. Even though great achievement has been made in solar flare forecasting based on these two factors, it is necessary to propose novel precursor factors reflecting the physical mechanism of solar flare eruptions and have a strong correlation with them to further improve the forecast accuracy.

The second key step is to preprocess the flare observation data before training a forecast model. Thus far, observation tools and measurement instruments under large-scale deployment provide massive flare data, and based on data-driven forecast models, a large amount of data can be used to train the models and obtain flare outburst patterns. However, there are non-negligible problems with the data preprocessing. On one hand, the space environment where the artificial satellite works, such as charged particles, radiation, and magnetic field, will induce noises in the flare observation data and images. On the other hand, as flare eruption is a small-probability event, flare events represent a minority class in the sample data. The imbalance phenomenon of flare sample data will bring difficulties with learning the flare outburst patterns of a minority class. Currently, most researchers use resampling to

resolve the class imbalance problem in the flare data. Nevertheless, resampling cannot fully use the effective information in the data, and it will introduce additional errors to the forecast models. Thus, it is urgent to investigate the preprocessing methods to attack the imbalance problem in flare forecasting.

The third and most critical step is to build a prediction model using statistical ML methods, deep learning methods, or a combination of them. Single and fusion models have advantages in forecasting tasks, and evaluation of the model performance requires a horizontal comparison and analysis of multiple quantified metrics. Overall, more attention should be focused on the model structure design and type selection. Meanwhile, choosing more novel algorithms and designing the models adapting to the imbalance problem are hot topics for future research.

Given the above problems in solar flare forecasting, we herein review the research status of flare forecasting from the following three aspects: selection of forecast factors, flare samples and their preprocessing methods, and design methods of the forecast model. In the first section, we introduce the classification information of the sunspots and evolution pattern of the magnetic field, and the historical flare rate based on the multiple evolution patterns of flares and their outburst correlations is discussed. The second section introduces flare samples and their preprocessing methods, mainly including the methods of standardization and normalization of samples and the methods of class imbalance processing of samples. The third section overviews the design methods of the forecasting model, in terms of the single model design methods, fusion model design methods, and other forecasting methods. The design methods of the single and fusion models are discussed with regard to shallow and deep model design, respectively. In the fourth section, current research status of solar flare forecasting is summarized, and its development trend is sketched. The article concludes in the last section.

2. Selection of Forecast Factors

Cicogna et al. (2021) pointed out that solar flares erupt in solar active regions, which host a complex and powerful bipolar magnetic flux. Estimating the probability of flare eruptions in the active regions and making a reliable forecast of them is challenging. The first step of forecasting a flare outburst is to select flare forecast factors. Selecting appropriate forecast factors is critical to improving the performance of flare-forecasting models. Most available flare forecast algorithms, both at the experimental and research stages, estimate future flare probabilities based on sunspot parameters of the active regions, magnetic field parameters, and historical flare rate.

2.1. Sunspot Parameters

Sunspots refer to dark spots in the solar photosphere, which have the characteristics of a strong magnetic field and low temperature; therefore, they appear black compared with the adjacent regions and are considered a good marker of the solar active regions. Sunspots' rotation (Vemareddy et al. 2016) and shear motion in the photosphere (Vemareddy et al. 2012) contribute to the accumulation of magnetic energy in the active regions (Démoulin & Pariat 2008), thereby providing conditions for flare eruptions. The direct observation quantities based on sunspots include the number of sunspots, number of sunspot groups, area of sunspot groups, longitudinal extension value of the solar surface, and morphological characteristics of the sunspot.

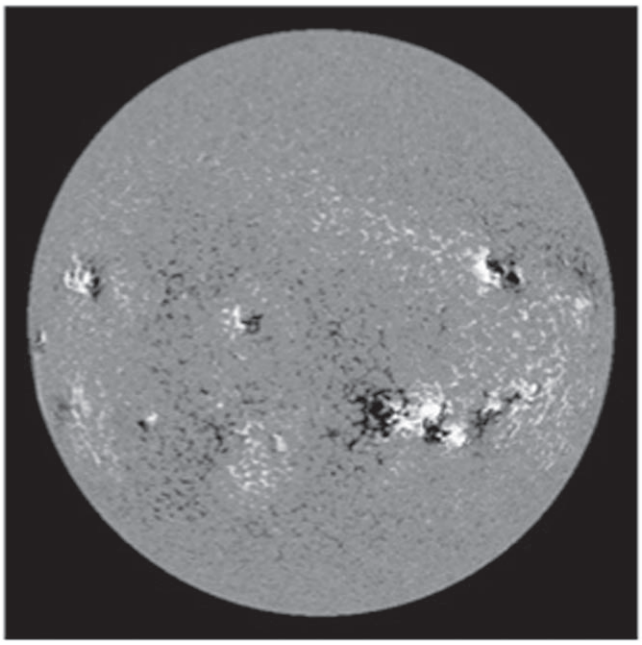

Figure 1. Active sunspot groups (flares will erupt within the next 48 hr).

The more complex the morphology and polarity of the sunspots are, the higher the likelihood of a flare outburst is. Figures 1 and 2 show two typical longitudinal magnetic maps of the full solar disk for clarifying this. With a reasonable classification of sunspots, researchers can better characterize flare events (McIntosh 1990). According to the magnetic field polarity and morphological characteristics of a sunspot, solar physicists have given the following three classification methods. In 1919, the Mount Wilson Observatory in the United States proposed the magnetic classification of Mount Wilson, classifying the sunspot groups into four types—α, β, γ, and δ—depending on their polarity (Hale 1908), and a sunspot group may correspond to multiple magnetic classifications simultaneously. In 1938, Zurich classification was proposed at the Zurich Observatory in Sweden (Carrasco et al. 2015), which classified the sunspots into nine types, denoted by A, B, C, D, E, F, G, and J, based on the development process of the sunspot groups' morphology. In 1990, McIntosh (1990)

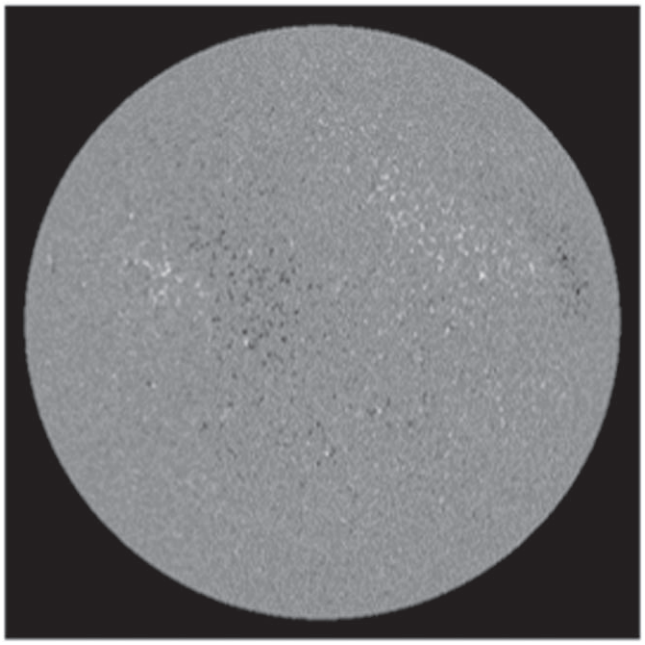

Figure 2. Tranquil sunspot groups (no flares within the next 48 hr).

improved the Zurich classification, using three letters to indicate the morphological categories to which a sunspot group belongs, and the first letter was simplified into seven types: A, B, C, D, E, F, and H. The second letter represents the morphological characteristics of the largest sunspot group, including six types: x, r, s, a, h, and k. The last letter characterizes the distribution of sunspots and is recorded as four types: x, o, i, and c. The commonly used classification criteria in current studies are the Wilson Mountain magnetic classification and the McIntosh classification.

2.2. Magnetic Field Parameters

The solar magnetic field is divided into the active region, polar region, and tranquility region magnetic fields. The main sources of the magnetic field parameters are the solar photosphere and chromosphere. The physical state, motion, and evolution of the Sun are closely related to the magnetic field, which is the direct driving source of solar activities such as sunspots and flares.

Gallagher et al. (2002) analyzed the relations between the photospheric magnetic field and flare. They found that active regions with higher flare eruption rates exhibit large and significantly changing magnetic-field gradients. Lim et al. (2019) developed a model for forecasting the daily outburst rate of M and X class flares based on the statistical relation between the photospheric magnetic field parameters and the daily flare outburst rate from 2010 May to 2018 April. The research of Cui et al. (2006) based on the full solar disk and vector magnetograms showed that the flare outburst rate is well correlated with a series of physical quantities describing the non-potential nature and complexity of the photospheric magnetic field, such as the maximum horizontal gradient of the longitudinal magnetic field. Komm & Hill (2009) observed that the vorticity and magnetic flux corresponding to the active regions of flares of different levels are quite different, with M-class flares related to large vorticity and X-class flares relevant to both large vorticity and large magnetic flux simultaneously.

Table 1
Physical Quantities Describing the Magnetic Field in the Solar Active Region

Name of Physical Quantity	Calculation Formula
Total photosphere magnetic field free energy density	$\rho_{\rm tot} = \sum(B^{\rm Obs} - B^{\rm Pot})^2 dA$
Mean value of free energy of photosphere magnetic field	$\bar{\rho} \propto \frac{1}{N}\sum(B^{\rm Obs} - B^{\rm Pot})^2$

Korsós et al. (2018) analyzed the evolution process of the active region before the flare eruption using SDO/HMI Debrecen data according to their proposed weighted horizontal magnetic gradient (WG_M) (Korsós et al. 2015) in 2015. By studying two typical active regions, it was observed that the WG_M and its time-series characteristics are strongly correlated with flare events. In addition, the evolution of magnetic helicity is closely related to flare outbursts. By analyzing three flare active regions and three non-flare eruption active regions, Korsós et al. (2020) observed that the evolution of magnetic helicity in the active region of a flare outburst has apparent periodicity and can be a valuable precursor of flare eruptions.

Li & Du (2019) used the vector magnetic field data of 12 months to extract four physical parameters as flare forecast factors, which are (1) the maximum horizontal gradient of the longitudinal magnetic field, (2) the length of the neutral line, (3) the number of singularities, and (4) the sum of the photosphere magnetic free energies $\rho_{\rm sum}$, where $\rho_{\rm sum}$ is calculated as follows

$$\rho_{\rm sum} = \sum(B^{\rm Obs} - B^{\rm Pot})^2. \quad (1)$$

The reference equations for calculation of $\rho_{\rm sum}$ are shown in Table 1:

Several observational studies have found that the polarity inversion line (PIL) (Gopalswamy et al. 2003) in the strong magnetic field region plays a vital role in flare activity (Louis et al. 2015) and is a critical forecasting factor for solar flares. Sadykov & Kosovichev (2017) confirmed the important role of PIL in flare eruption and experimentally verified the possibility of using only line-of-sight magnetograms for flare forecasting. Yi et al. (2021) proposed a flare forecasting model based on a convolutional neural network (CNN) and the morphological interpretation of PIL related to the physical parameters of the solar active region. They consider PIL to be an essential

predictor for training flare forecast models using deep learning methods.

The New Scientist website reported on 2020 July 30 that Kusano et al. (2020) at Nagoya University in Japan developed a physical model known as the kappa scheme that can forecast the outburst of solar flares several hours in advance. The timing, location, and scale of flare eruptions depend mainly on the magnetic flux density close to the solar surface PIL. The kappa scheme makes predictions by analyzing strong magnetic fields related to solar flares. Using the kappa scheme, the exact location and scale of each flare outburst can be clarified, and the feasibility of the sunspots and magnetic field evolution characteristics in the active region as flare forecasts can be indicated.

Thus, the magnetic field parameter is becoming an important forecasting factor owing to its clear physical meaning.

2.3. Historical Flare Rate

Flare outbursts are small-probability events, and their eruption is strongly periodic and characterized by localization. Park et al. (2020) inferred that the key to successfully forecasting the timing of a flare eruption is to focus on the transition period between the calm and active phases of the flare, and they proposed a method of combining forecast factors to evaluate the accuracy of the prediction. Experiments have shown that for flare outbursts of M level and higher, considering temporal accumulation or periodicity in the prediction process helps improve the overall flare forecast performance. In terms of selection of flare prediction factors, the attention mechanism (Niu et al. 2021) can be used to select the features that are more critical to flare forecasting among the input features, thus improving the prediction rate of the model. Park and Leka improved the accuracy of their model in forecasting flare outbursts. However, the time cost of model training is ignored, while a model incorporating the attention mechanism can make fast classification predictions even though it sacrifices some accuracy.

Roy et al. (2020) studied the short and long-term fluctuations of the solar chromosphere using flare forecast factors. At first, they obtained data from the Northern Hemisphere, Southern Hemisphere, and the entire flare period from 1976 January to 2014 December, portraying the periodicity of the flare outbursts. Wheatland (2004) used the historical information on flare eruptions in active regions in the forecast model. They obtained a high accuracy rate for the X-class flares. Nishizuka et al. (2017) considered flare observation data from 2010 to 2015 and extracted 60 flare-related features, including the magnetic neutral line, current helicity, and historical flare rate. They employed three ML algorithms for flare forecasting: support vector machine (SVM), k-nearest neighbor (KNN), and random tree. The experiments show that using the historical flare rate as a forecasting factor can improve flare forecast performance.

2.4. Other Parameters

In addition to the above common forecasting factors, several other types of forecasting factors have been proven to be feasible for forecasting flares. Aschwanden & Aschwanden (2008) investigated the correlation between the fractal dimension of specific indicators of flare outbursts in active regions and flare eruption rates according to the fractal approach of nonlinear science. Yu et al. (2009) proposed the concept of a combination of forecasting factors based on the rough set theory to select the essential forecasting factors. They solved the problem of excessive dimensionality while retaining as much information as possible regarding the data.

The solar 10.7 cm radio flux correlates well with flare outbursts, and the phenomenon of a sudden increase in radio flux is called a radio burst. Ndacyayisenga et al. (2021) performed a statistical analysis of radio bursts and explored their relations with the number of sunspots. Experiments have demonstrated that radio bursts are closely related to the number of sunspots, and statistical analysis of radio bursts has observed that 65% of them are related to flare events. Panos & Kleint (2020) thought that the photospheric magnetic field data could not completely meet the data source of flare prediction, and they extended the study of flare prediction to spectral data for the first time. Research has shown that well-performing flare prediction models can be generated from spectral data alone, thereby confirming the feasibility of using spectral data for flare prediction. Gyenge et al. (2016) studied the temporal and spatial properties of flare eruptions and demonstrated that they can be used to improve the accuracy of flare forecasts.

Space satellite observations conducted by Skylab, the Solar Maximum Mission (Doschek 2021), and the Yohkoh (Sharma et al. 2021) project in Japan have identified several new characteristics of flare outbursts. According to the features of the flare outbursts found, we can extract flare-related forecasting factors: the density of the coronal layer which increases by one to two orders of magnitude as the accelerated particles release heat at the location of flares in the coronal layer, and then moves toward the interior of the Sun to reach the chromosphere. In the chromosphere, the heat released by the particles increases the temperature of the plasma gas and expands it into a plasma ring through evaporation. Subsequently, the toroidal plasma is cooled by energy conduction and radiation and flows back to the bottom of the magnetic lines of force, i.e., the coronal layer. By imaging the X-ray, we observe that the X-ray is usually emitted from the bottom of the flare in the flash phase. Starting from the pre-flare phase, the coronal streamers covering the flare are generally ejected in the form of bubbles and are known as coronal mass ejection (CME).

2.5. Section Summary

The first step in flare forecasting is selecting the forecast factors. Using appropriate forecast factors can significantly improve the performance of flare-prediction models. In this section, research on flare predictors in recent years is in terms of sunspot parameters, magnetic field parameters, historical flare rate, and other parameters. As the fractal information of the sunspots and evolution pattern of the magnetic field have a strong correlation with the flare outbursts, they were used as the preferred forecast factors. Although other parameters have a certain correlation with the flare outbursts and are utilized as forecast factors in some studies, their validity still needs to be verified through a large number of experiments.

3. Flare Samples and Their Preprocessing Methods

3.1. Normalization and Standardization of Flare Samples

3.1.1. Sample Normalization Process

Because different forecasting factors in the solar flare data set have different dimensions and orders of magnitude, the effectiveness of models that require kernel functions, such as an SVM, can strongly depend on whether the features are normalized. When the order-of-magnitude difference between individual features is significant, if the original metrics are directly input into the model, the features with a larger order of magnitude are dominant in the kernel function calculation. By contrast, features with smaller values are ignored, which is likely to lead to a large amount of information loss. Therefore, to guarantee the reliability of the results, original features must be normalized.

The most common method of normalization is min-max normalization. The principle is to calculate the ratio of the difference between each original data value and the minimum value to the sample value interval length. Afterward, all data values are transferred to the [0, 1] interval, where x and x' represent the samples before and after scaling, respectively, and $x_{\min}$ and $x_{\max}$ represent the minimum and maximum values of the samples, respectively. This is expressed by the following equation

$$x' = \frac{x - x_{\min}}{x_{\max} - x_{\min}}. \tag{2}$$

3.1.2. Sample Standardization Process

The standardized method is used for preprocessing, as shown in Formula 3, where μ and σ denote the mean and standard deviation, respectively, of the sample data. The mean of the transformed sample data is 0 and the variance is 1, which mitigates the effect of sample outliers on the scaling results to a considerable extent.

$$x' = \frac{x - \mu}{\sigma}. \tag{3}$$

Standardization accelerates the model update weights and convergence effectively and improves the accuracy of the forecast model.

3.2. Class-imbalance Processing Methods of Samples

3.2.1. Inter-class and Intra-class Imbalances in Flare Samples

Imbalanced data is a general term for data with imbalanced sample sizes or different misclassification costs (Vuttipittayamongkol & Elyan 2020). As the forecast model was initially designed for the classification of balanced data sets, when it is used for classifying imbalanced data sets, it usually tends to favor the majority of class samples. This may render the classifier unable to learn the pattern of a few classes of samples and accurately classify them, resulting in degraded classification performance (Tao et al. 2019). In addition, an imbalance problem was also present in the training set of the flare forecast models. That is, flare eruption events are small probability events corresponding to a small number of classes in the data set, and dealing with class imbalance problems is necessary.

The imbalanced state of the data set can be subdivided into two types: inter-class and intra-class imbalances (He & Garcia 2009), as shown in Figure 3. Among them, inter-class imbalance refers to an imbalance in the number of samples between various categories in the data set. Intra-class imbalance refers to the imbalance of data distribution density within a certain class of sample space. That is, there are multiple subcategories with the same category and different data distributions.

The frequency of flare outburst varies with the solar cycle showing a periodicity of about 11 yr, and the number of flare outbursts is significantly more in the active period than in the quiet period (Nandy 2020). Therefore, the intra-class imbalance problem also exists in the flare samples, but most of the current studies focus on the impact of the inter-class imbalance problem in the flare samples on the model forecast accuracy. We herein mainly overview the processing methods of the inter-class imbalance in flare samples.

3.2.2. Class-imbalance Processing Methods Based on Resampling

Resampling methods for solving class imbalance (Batista et al. 2004) generally include oversampling, undersampling, and mixed sampling. The resampling method is at the root of solving the class imbalance problem directly from the data level and is not constrained by a specific classification model (Yu et al. 2018). Figure 4 illustrates the basic principle of resampling.

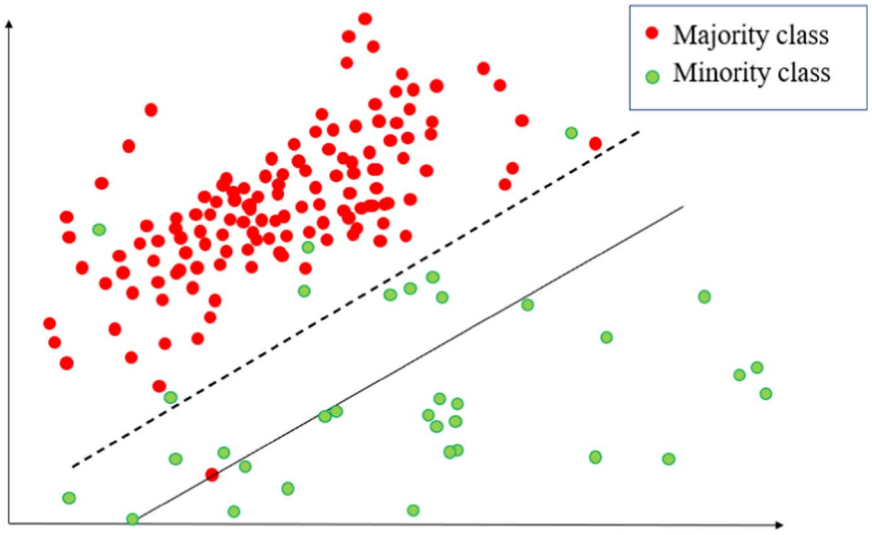

Figure 3. Inter-class imbalance and intra-class imbalance.

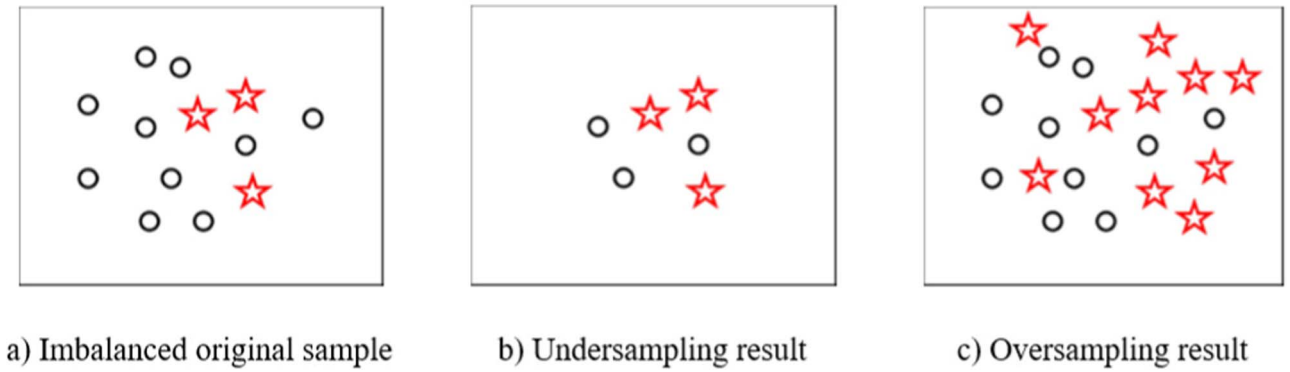

Figure 4. Basic principle of resampling.

Oversampling aims to increase the number of minority-class samples to achieve a reduction in sample imbalance, whereas undersampling has the opposite effect. Mixed sampling is a neutralization of the individual oversampling and undersampling methods. However, traditional oversampling or undersampling methods simply change the number of samples to a balanced ratio. The undersampling methods may lead to loss of sample information and the oversampling ones may cause artificial errors. Meanwhile, they introduce additional errors to the model if the information in the data is not fully utilized.

Most studies use a resampling-based approach to dispose of the class imbalance in flare data. Table 2 shows the classical algorithms for resampling methods and their characteristics.

3.3. Section Summary

The problems of redundant attributes, class imbalance and noise in solar flare observed data can greatly reduce the speed of flare model training and the accuracy of forecasting. Therefore, to improve the training efficiency and accuracy of the prediction model, preprocessing the flare observation data is necessary. This section first briefly introduces the normalization and standardization of flare data, and then reviews the class imbalance processing methods based on resampling in flare forecasting in recent years. Currently, most studies use resampling to address class imbalance problems in flare data. However, resampling methods cannot fully use the valid information in the data and they may introduce additional errors to the forecast models. Therefore, several studies have started to consider and experiment with a range of classifier-based imbalance processing methods, such as methods of classifiers incorporating resampling strategies, methods of classifiers with the introduction of cost-sensitive factors, and methods of classifiers based on regular term optimization. However, these methods have not

Table 2
Resampling Methods and Their Main Characteristics

	Method Name	Characteristics
Undersampling	Plain undersampling	Random removal of negative samples; Simple and more random.
	Clustering-based undersampling	New negative samples are generated based on clustering, which better retains the information of the original negative samples.
Oversampling	Plain oversampling	Random replication of positive samples; Simple and more random.
	(Chawla et al. 2002) SMOTE	Based on distance, positive samples are generated by linear interpolation, which helps to reduce the risk of overfitting.
	(Han et al. 2005) Borderline-SMOTE	More boundary information is considered than SMOTE, and the synthesized samples are more closely concentrated at the category boundaries.
	(Beinecke & Heider 2021) ADASYN	The variant of SMOTE; The synthetic positive samples mostly originate from minority positive samples that are closer to the negative samples.
	Clustering-based oversampling	New positive samples are generated based on clustering, and the characteristics of the original positive samples are refined.
	(Wang & Duan 2017) DS-SMOTE	Based on the distance, the density threshold is calculated to obtain the sparse combination, and the linear value is obtained.
Mixed sampling	(Arjun & Manoj 2021) SMOTE-ENN	Use data cleaning technology to solve the problem that SMOTE often produces overlapping samples.
	(Wang et al. 2019) SMOTE-Tomek	

been widely used in flare forecasting, and their applicability needs further investigation.

4. Design Methods of Forecasting Model

Flare prediction models based on ML algorithms rely mainly on information such as sunspot morphology and magnetic field evolution parameters extracted from the solar active regions or collected from the satellite observation sites and observations in observatories (Nurzaman & Dani 2019). The core of the forecast models is to establish the complex nonlinear correlations between the flare outburst and the chosen parameters. So far, many researchers have explored and designed models with high forecasting rates.

According to their structural properties, the models are classified as static, dynamic, or self-organizing (Osokin et al. 2004). Output of the static model is only related to input at the current moment, i.e., it portrays the flare situation during the forecast period from the observations in the current moment. Compared with a static model, a dynamic model introduces information on the evolution of the active region, i.e., based on the current state of the active region, influence of the previous state of the active region is also considered. The self-organizing criticality model is based on the theory of self-organizing criticality that assumes that when the system is in a critical state the behavior of all its components is interrelated. In flare activities, this is reflected in the magnetic reconnection events, which cause the magnetic field gradient to be less than the critical state value by releasing the magnetic field energy. When a new magnetic field vector is added, the process is repeated, eventually driving the magnetic field to a critical state, which in turn leads to a flare outburst. Compared with the first two models, the physical interpretation of this class of models is better (Morales & Charbonneau 2016).

4.1. Design Methods of a Single Model

4.1.1. Design Methods of Shallow Model

Liu et al. (2017a) trained a flare forecast model based on a random forest (RF) using the physical parameters provided by the SDO/HMI active region patch (SHARP). Based on the maximum radiation intensity produced by the X-ray flares, they divided the active regions of flare eruptions into four categories to predict the eruption probability of a certain type of flare in a given active region within 24 hr. The experiments showed that the RF forecast model trained with the SDO/HMI parameters has a fairly high forecast rate. This is the first time that RF has been used to make multiclass forecasts of solar flares. In the same year, Liu et al. (2017b) used a model trained by RF to forecast the eruption of flares with a specific intensity level within 24 hr for a given active region. Through analysis of the soft X-ray emission data observed during the current solar activity minimal period from 2017 July to September, Stanislavsky et al. (2019) showed that the eruptive or non-eruptive state of the solar flare conforms to the hidden Markov model (HMM) (Stanislavsky et al. 2020). In the following year, they proposed a statistical method for predicting soft X-ray flare outbursts using the HMM, which also achieved higher accuracy in flare forecasting.

Falco et al. (2019) described a flare forecasting tool based on sunspot group characteristics, assuming that the frequency of flare eruptions follows Poisson statistics. The tool uses observational instruments to collect the morphological attributes of sunspot groups and then calculates the probability of flare outbursts in active regions. This tool, which combines

sunspot morphological parameters and statistical techniques, has a high forecast rate and is more sensitive to flare eruptions with high strength levels. To further improve the accuracy of flare forecasting, Yuan et al. (2016) proposed a flare forecast model combining principal component analysis (PCA) and SVM and comprehensively considered forecast factors such as sunspot parameters and 10.7 cm solar radio flux. They first coded the above parameters with appropriate attributes and normalized the data set for preprocessing. Subsequently, they extracted the main features using PCA and applied SVM to build the forecast model. Finally, they made a horizontal comparison between their model and the model combines photospheric magnetic field parameters and sunspot parameters in the active regions which was proposed by Rong et al. (2013). The analysis showed that the model has a strong ability to predict positive cases, a higher accuracy rate (AC) and a lower false alarm rate (FAR).

Jonas et al. (2018) used ML methods to extract relevant magnetic field evolution information from the photosphere and coronal observational images to build flare forecasting models. Florios et al. (2018) used various ML algorithms, including RF, multilayer perceptron (MLP), and SVM, to establish flare-forecasting models. The ML-based forecasting model pipeline design was defined by Cinto et al. (2020). It is divided into five steps: feature selection, hyperparameter update and optimization of the model, model loss function selection, adjustment of the model training endpoint, and model performance evaluation. Subsequently, a flare forecasting model based on an extreme gradient enhancement tree and considering time-series features is established to verify the validity of that standardization. The evaluation indexes of the model show that the model has a higher true skill score (TSS) and a lower FAR than other basic models.

Domijan et al. (2019) established a flare-forecasting method based on the characteristic magnetic parameters generated by a solar active region detection tracker (SMART) (Higgins et al. 2011). They used edge correlation as a feature selection method to establish magnetic features related to the flare eruption intensity and designed forecasting methods by deducing flare eruption patterns through logistic regression. Anastasiadis et al. (2017) attempted to reveal the complex mechanism of flare outbursts and thus predict solar flare events by statistically analyzing a large number of magnetic maps of active regions. Ma et al. (2017) used univariate clustering combined with multivariate decision trees for flare prediction based on incorporating time-series features of flare data sets. They observed that the total unsigned magnetic flux and total unsigned magnetic helicity were strongly correlated with flare outbursts compared to other characteristic parameters. Hazra et al. (2020) used photosphere magnetic parameters and their time-series characteristics to train a logistic regression algorithm to forecast solar flares. The magnetic parameters included the total unsigned magnetic flux and total unsigned magnetic helicity. Finally, the experiments show that the model has a higher TSS than other classifiers under the same conditions.

4.1.2. Design Methods of Deep Model

Macroscopically, analyzing the morphology and evolutionary characteristics of solar active region parameters is an essential means of predicting solar flare eruptions. Classical flare forecasting models are established based on statistical relations between solar flares and forecast factors extracted from observational data. The artificial method of extracting solar activity features cannot meet the requirements of flare forecasting. In this regard, Li & Huang (2018) used an ML algorithm to extract the corresponding flare forecast factors to establish a forecast model. Using three forecast factors extracted from longitudinal magnetograms of the full solar disk, Wang et al. (2017) adopted a neural network algorithm to build a short-term forecast model for flares. The model forecast accuracy was comparable with that of a professional with long-term forecasting experience. Nishizuka et al. (2018) developed a forecasting model called the Deep Flare Network (DeFN), using deep neural networks (DNNs), that overcomes the challenge of a traditional DNN forecasting process as a black box (Castelvecchi 2016).

Huang et al. (2018) proposed a CNN-based model for solar flare forecasting that uses images of the active regions within 30° selected from SOHO/MDI and SDO/HMI magnetograms to train and test the CNN. They indicated that this model focuses on active-region magnetograms with PIL or strong magnetic fields. Based on the improvement of the CNN algorithm, Fu et al. (2018) attempted to forecast solar flares using a LeNet-5 type of CNN. The model is characterized by stacking convolutional and pooling layers to capture complex abstract features in image data. Deshmukh et al. (2020) used CNN to extract the morphological features of images and combined them with manually extracted features for flare forecasting using MLP. Experiments show that the method is more accurate than forecasting methods that use a single feature. Abed et al. (2021) established the ASAP_Dep flare prediction model by integrating CNN and Softmax classifiers based on the ASAP system introduced by Colak & Qahwaji (2009), where the model extracts special features from SDO/HMI images. The experiments showed that the model performed better on the FAR, TSS, and Heidke Skill Score (HSS). Shin et al. (2016) proposed an AlexNet architecture based on CNN to construct flare-forecasting models using SOHO/MDI images. For class C, M and X flares, the accuracy of the model to predict flare bursts is 90%, of which the accuracy of class M and X flare bursts is 96%, and the FAR is 60%. Deng et al. (2021) balanced the number of samples for different flare strength levels using generative adversarial network (GAN) technology. The experiments showed that sample balance is crucial to the stability of the CNN model.

Table 3
Performance Metrics of the three CNN Models Compared with the Other Three Flare Forecasting Models

	ACC	FAR	HSS	TSS	Datasets
Lu et al. (2018)	0.78	0.14	0.57	0.57	
Khan et al. (2019)	0.79	0.21	0.57	0.56	Train: 1996–2008 Test: 2009–2017
Park et al. (2018)	0.82	0.17	0.63	0.63	
Colak & Qahwaji (2009)	0.81	0.30	0.51	0.47	Train: 1972–1998 Test: 1999–2002
Bloomfield et al. (2012)	0.71	0.65	0.32	0.46	Train: 1988–1996 Test: 1996–2010
Hunter et al. (2018)	0.76	0.65	0.34	0.49	Train: 1996–2010 Test: 2010–2015

That is, the augmented data generated by the GAN effectively improves the stability of the prediction model.

Park et al. (2018) used three CNN architectures to construct flare forecasting models, including AlexNet (Lu et al. 2018) and GoogLeNet (Khan et al. 2019), and they proposed a new model combining GoogLeNet and DenseNet (Huang et al. 2016). They used SOHO/MDI magnetograms from 1996 May to 2010 December to train the models and then used SDO/HMI magnetograms from 2011 January to 2017 June to test the models. The three CNN models were compared with the flare forecasting models proposed by Colak & Qahwaji (2009), Bloomfield et al. (2012), and Hunter et al. (2018) in the same data sets. Table 3 shows the comparison results of the models, among which all indicators of the CNN model proposed by Park, except FAR, are better.

Landa & Reuveni (2022) proposed a multilayer, one-dimensional CNN forecast model with time-series data of soft X-rays observed by the GOES satellite as the data set. The model was trained and evaluated by randomly selecting a portion of the data set and extracting time-series features. Experiments show that the model considering the time-series characteristics of the flare data has a higher forecast rate, and this makes recurrent neural networks (RNNs) and their corresponding variant algorithms, which can extract time-series features of data, a hot topic of research for researchers. In the study of RNN variants of long short-term memory neural networks (LSTMs) for short-term forecasting models of solar flares, Chen et al. (2019) used a self-encoder to extract features from SDO/HMI magnetogram data, and used LSTM to extract time-series features from the data for flare forecasting. Liu et al. (2019) utilized SHARP data to construct flare forecasting models for intensity levels $\geqslant$ M5.0, $\geqslant$M and $\geqslant$C in the next 24 hr, separately, based on the LSTM method considering historical flare rates.

He (2021) used the SHARP data provided by SDO/HMI in the active solar regions as a data set. They first analyzed the feature importance of each physical parameter in the SHARP data using the extreme gradient boosting (XGBoost) method (Ramraj et al. 2016). Subsequently, they extracted the time-series features of flare data and built the flare forecast model for the next 48 hr. The experiments show that the model is superior to the traditional ML models in terms of the true positive rate (TPR) and TSS, which are 0.7483 and 0.7402, respectively, and the FAR and ACC are close to those of the traditional ML models, which are 0.0081 and 0.9894, respectively. In general, the overall performance of the model was better than that of the traditional ML model. She compared this model with the CNN-based flare prediction models built by Li et al. (2011) with SOHO/MDI magnetograms as the data set and by Huang et al. (2010) using SOHO/MDI and SDO/HMI magnetograms as the data set for a horizontal comparison of quantified performance metrics. As shown in Table 4, compared with the CNN model using magnetogram data, the LSTM model has a slightly lower TPR than the CNN model, lower FAR than the model proposed by Huang, higher TPR than the model proposed by Li et al. (2011), and better accuracy (ACC) and FPR than the CNN model. Moreover, as shown in Table 5, the data samples of the LSTM forecasting model are fewer than those of the CNN forecasting models. The model performance can be further improved if the number of data samples in the LSTM forecasting model is increased.

Table 4
LSTM Model and CNN Model Evaluation

Forecasting method	TPR	FPR	FAR	ACC	TSS
He (2021) LSTM	0.7483	0.5000	0.0081	0.9894	0.7402
Li et al. (2011) CNN	0.8050	0.2297	0.1860	0.7919	0.6190
Huang et al. (2010) CNN	0.8100	0.8449	0.1900	0.8111	0.6200

Table 5
Contingency Table

Forecasting Method	True Positive (TP)	False Negative (FN)	True Negative (TN)	False Positive (FP)
LSTM	113	38	13840	113
CNN	1008	291	978	231
CNN	1614	378	37711	8783

4.2. Design Methods of the Fusion Model

4.2.1. Design Methods of Shallow Model

Considering the solar projection effect, most forecast models focus only on active regions within 30° of the center of the

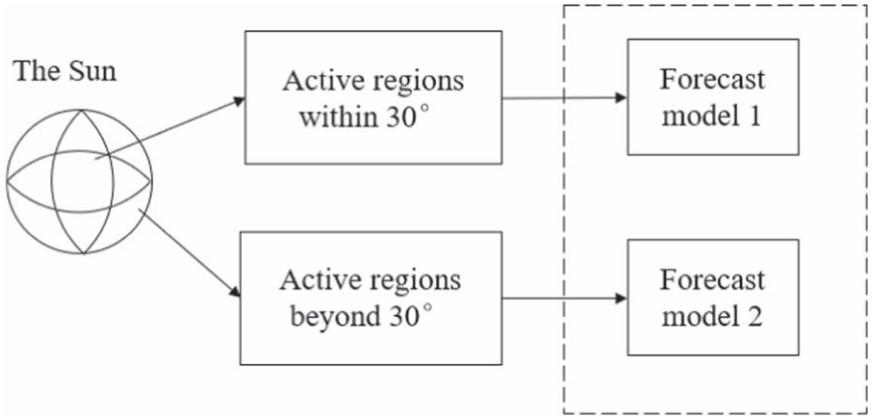

Figure 5. Full-disk solar fare forecasting model.

Table 6
Results of the Best Forecast Model in the Test Dataset of Solar Flare Forecasting

Time Range	Forecasting Model	Metrics			
		TP rate	TN rate	TSS	F1−score
24 hr	Majority voting method	81.0 %	77.4%	58.4%	49.4%
48 hr	RF and LightGBM	76.7%	74.8%	51.5 %	47.1%
72 hr	Majority voting method	81.2%	73.3%	54.5%	52.2%

solar disk. However, solar flares can also erupt in active regions outside 30°. To address this problem, Li & Du (2019) proposed a cost-sensitive decision tree algorithm. They built two flare forecasting models from the active regions within 30° of the solar disk center and outside 30° of the solar disk center. After evaluating the performance of the two models, they integrated them into one model, i.e., a full-disk solar flare forecasting model was obtained. The structure of the model is illustrated in Figure 5. The analysis shows that the forecasting rate of the model outside 30° of the center of the solar disk is worse than that of the model within 30°, owing to the projection effect. In addition, the model within 30° had a higher TN rate than the model built based on CNN under the same conditions. Benvenuto et al. (2020) combined supervised regression methods incorporating regularization with the classification techniques of unsupervised fuzzy clustering for flare forecasting. Subsequently, they compared the model with several single ML models under the same data set for analysis. The results show that the forecast performance of the hybrid method is better than that of all other unsupervised methods.

The ensemble forecasting strategy has been applied to numerical weather forecasting in recent years, and it is a method that combines different forecast models to obtain more accurate results. In the field of flare prediction, Guerra et al. (2016) demonstrated the applicability of ensemble forecasts with multiple model inputs for forecasting flare eruptions within a specific solar activity region. Ribeiro & Gradvohl (2021) analyzed three flare prediction methods: SVM, RF, and Light Gradient Boosting Machine (LightGBM) (Zhou et al. 2002). To uncover the best-performing combination of forecast models, they combined the three algorithms two-by-two through logical connectors. In addition, the three algorithms were combined by the majority vote combination method (Sun & Li 2008). Based on these combinations, the forecasting models of M-class and X-class flares within the time ranges of 24, 48, and 72 hr in advance are established. In addition, they highlighted the effect of data preprocessing on the performance of solar flare forecasting models. Table 6 displays the combination of forecasting methods with the best performance metrics on the test set at 24, 48, and 72 hr. The table shows that the majority vote combination method has good prediction performance at 24 and 72 hr. The above results affirm that the best approach to predicting solar flares is to combine the two approaches or the majority vote combination method.

Liu et al. (2017c) used the longitudinal magnetograms provided by SOHO/MDI and the magnetograms observed in the active regions to build image libraries, and they proposed a genetic optimization algorithm based on image libraries to infer flare outburst patterns. This inference method combines flare forecast results with the forecaster's experience to generate the final results. The experimental results show that the metrics of TP rate, HSS, and average accuracy of the method are better than those of the traditional ML methods. In particular, this method is the first to incorporate artificial experience to predict

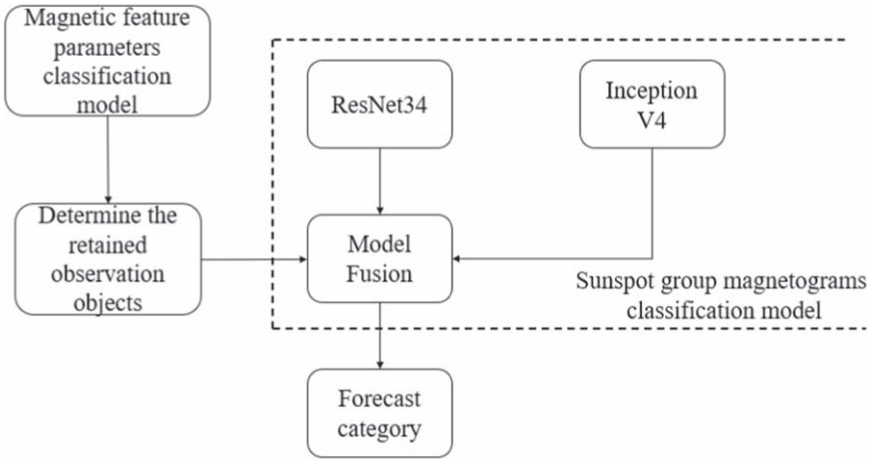

Figure 6. Structure of multimodal flare forecast model.

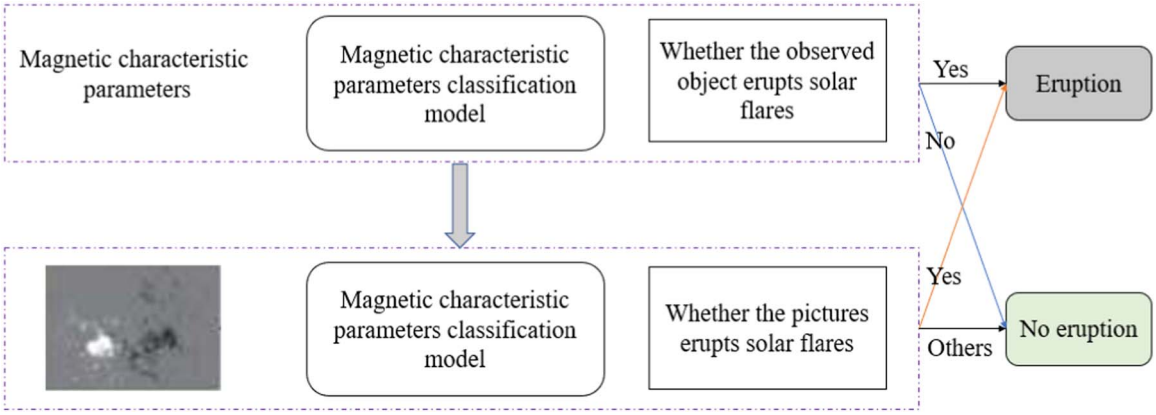

Figure 7. Schematic of model fusion strategy.

flare outbreaks. Murray et al. (2017) also highlighted the impact of incorporating artificial empirical forecasts into forecast models and demonstrated that models incorporating artificial experience had higher forecast rates than the original models. Park et al. (2017) proposed that the indicator scores for assessing the performance of flare forecasting models do not consider the effects of various cost losses. For the first time, they applied the indicator score-based decision to a flare prediction model with cost loss.

4.2.2. Design Methods of Deep Model

Based on the deep learning method, a multimodal flare forecasting model was proposed by Ma et al. (2021). By combining the active region magnetograms, magnetic field parameters, and flare event labels with the advantages of high accuracy of fully connected neural networks, high recall of CNN, and its ability to effectively extract high-level semantic information, they trained flare prediction models based on the sunspot group magnetograms as well as the magnetic feature parameters, separately. Finally, they formed the final output by the weighted fusion of the forecast results of the two models. The fusion model structure is illustrated in Figure 6, and the results of the discriminative strategy are depicted in Figure 7. The experiments show that the main performance evaluation metrics of the model were at least 7.8% better than those of the other models. Table 7 presents a horizontal comparison of the quantified metrics of the performance of the forecast models designed by Yuan et al. (2016), Ma et al. (2021), and He (2021).

Deng et al. (2021) proposed a hybrid CNN model for global flare forecasting, and the model was denoted as M. Considering the effects of the rising and falling phases of the solar activity cycle, they proposed two CNN sub-models—M_{rp} and M_{dp}—for forecasting flare outbursts in the rising and falling phases of the solar activity cycle, respectively. The experiments show that the TSS of model M improved considerably compared with

Table 7
Horizontal Comparison of Flare Prediction Models by Yuan, Ma, and He

	Horizontal Comparison	ACC	Recall	FPR	FAR
Yuan et al. (2016)	MLP	77.9%	68.1%	22.1%	···
	PCA-SVM	82.7%	62.9%	17.3%	···
Ma et al. (2021)	Sigmoid	89.3%	41.1%	···	34.7%
	CNN(ResNet34)	88.4%	37.1%	···	26.3%
	CNN(Inception V4)	90.4%	41.1%	···	59.2%
	Multimodal model	94.5%	41.1%	···	59.7%
He (2021)	LSTM	93.94%	74.83%	50.00%	···
	XGBoost	91.96%	50.66%	48.99%	···
	SVM	91.99%	32.45%	45.56%	···
	RF	90.91%	31.78%	54.28%	···

those of previous studies; in particular, the TSS of the two sub-models was higher. Zheng et al. (2019) proposed a hybrid CNN four-classification model wherein the intensity level of flare eruptions can be predicted. The model comprises three binary classification sub-models with similar structures, one of which coarsely classifies the sample inputs and the other two sub-models of which then finely classify the classification results of the first stage. This strategy effectively reduces the additional error in the model caused by the imbalanced sample numbers of the flare outburst categories (N, C, M, and X). The overall structure of the model is shown in Figure 8.

Chen et al. (2022) proposed a two-stage flare forecasting system, the first of which consists of an unsupervised clustering algorithm, k-means, which was used to improve the TP rate, and several CNN models, which improved the flare forecasting rate by integrating the forecasting results of the CNN models. In the second stage, three CNN models were selected: Xception, Resnet18, and Resnet34. The results demonstrate that the F1–score of this flare forecasting system reaches 0.5639. Deshmukh et al. (2022) proposed a hybrid two-stage ML method to alleviate the problem of high FAR in flare forecasting models. The first stage is a CNN model based on the VGG-16 structure and the second stage is a model based on an extreme random tree (ERT). In model training, the hyperparameters are updated iteratively to maximize TSS, which solves the problem of large discrepancy between the TP and FP rates in the highly imbalanced flare data set. Finally, they established a flare forecast system 12 hr in advance.

Sun et al. (2022) used data sets from two solar observation cycles provided by SMART and SHARP (Bobra et al. 2021) to examine the flare forecasting performance of two deep learning models—LTSM and CNN models—and explored the possibility of combining LSTM and CNN. The experiments showed that LSTM generally performs better than CNN forecasts as the sample size increases considerably for two solar cycles. In addition, the fusion model of the LSTM and CNN has a higher TSS than the individual models.

Making a series of optimizations and building a flare prediction model based only on CNN does not essentially solve the problem of simply using image recognition and ignoring the fact that flare samples have time-series characteristics. In this regard, Fang (2018) proposed fusing LSTM to extract the time-series characteristics of flare observed data of active regions based on a CNN, and the structure of the fusion model is illustrated in Figure 9. Analysis of the prediction results showed that the fusion model achieved 94.1% accuracy, 94.6% precision, 87.5% recall, 91% F1−score, 86.6% HSS, and 85% TSS. This model was compared with the models based on multi-model fusion proposed by Liu et al. (2017b) and the models designed using shallow neural networks proposed by Li & Du (2019) under the same conditions, as affirmed in Figure 10. Wan et al. (2022) designed a resampling-based CNN and Gated Recurrent Unit (GRU) fusion model for flare forecasting and showed that the fusion model has an advantage in flare forecasting tasks, i.e., by comparing the forecast performance of a single algorithm and the fusion algorithm, the TSS, HSS, and FAR of the fusion algorithm are superior. Table 8 displays a horizontal comparison of the quantified metrics of the flare prediction models of Fang (2018), Li & Du (2019), and Wan et al. (2022). Tang et al. (2021) used the observed magnetograms of sunspot groups and a neural network method driven by characteristic magnetic parameters to design a flare prediction model that incorporated DNN, CNN, and bidirectional LSTM. The experiments confirmed that the fusion model outperformed traditional statistical models and any single ML model.

4.3. Other Forecasting Methods

Sunspot activity directly affects the outer space environment, and flares erupt when they gather to a certain level. The least-squares support vector machine (LSSVM) (Suykens et al. 2002) can effectively solve the highly nonlinear problem of forecasting the monthly mean sunspot numbers, providing a new idea for flare forecasting.

When a flare erupts, a large number of X-rays are the first to reach the Earth, causing a sharp increase in the electron concentration in the ionosphere, resulting in a subsequent decrease in the equivalent reflection height of the ionosphere, which causes a phase anomaly in the very-low-frequency (VLF) signal. Su et al. (2019) used a VLF receiver to monitor the abnormal phase changes of the VLF signal during the launch of the Chinese “Shenzhou-1” spacecraft. Subsequently, the intensity level of the flare was successfully predicted based on these data and compared with the flare eruptions observed by the GOES satellite managed by the U.S. The results show

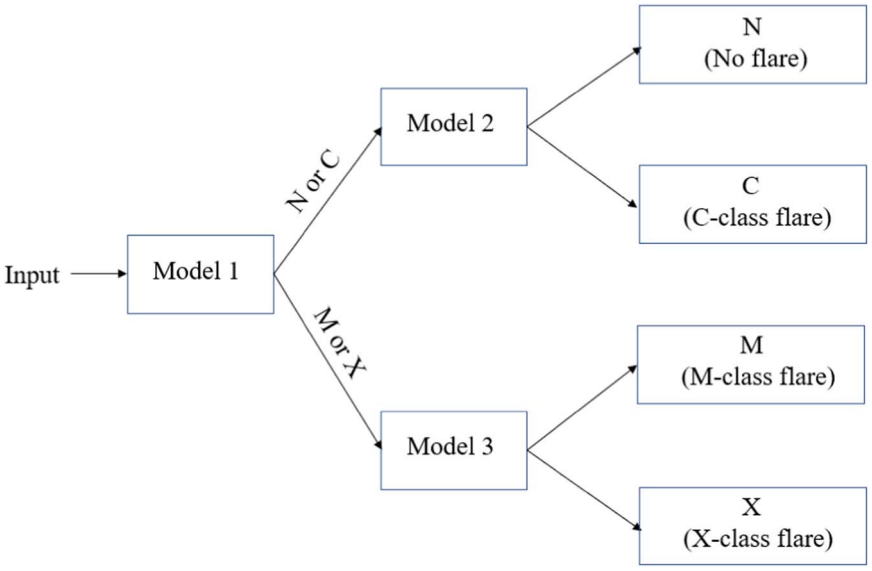

Figure 8. Overall structure of the hybrid CNN-based four-classification model for solar flare prediction.

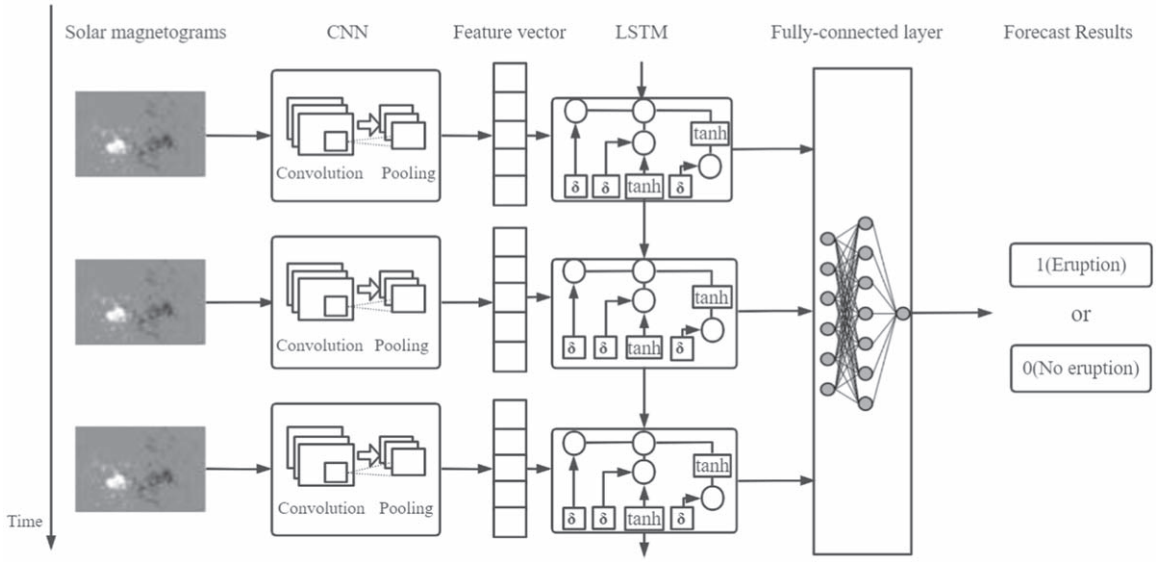

Figure 9. CNN+LSTM fusion forecasting model structure.

that the prediction is highly consistent with the GOES satellite observations of flare outbursts, which verifies the feasibility of the VLF method for forecasting solar flares. Flare eruptions are characterized by enhanced X-ray fluxes, and the direct forecasting of X-ray fluxes can reflect flare outbursts to some extent. Yi et al. (2020) forecasted the X-ray flare flux profile by designing a deep-learning model. The results show that the model can successfully perform distribution forecasting of flare X-ray flux without any preprocessing of the data to extract features and outperforms other models.

Krista & Chih (2021) introduced a flare eruption tracking tool that identifies flare characteristics and outburst precursors by detecting extreme ultraviolet (EUV) radiation values, revealing the relation between EUV and flares and the possible mechanisms causing flare eruptions. In addition, Bertolucci et al. (2017) and Edmonds (2018) studied the relations between planetary positions and flare outbursts. Petrakou (2021) investigated the relations between the timing of flare eruptions and the relative motion of planets and used ML techniques to forecast flare outbursts.

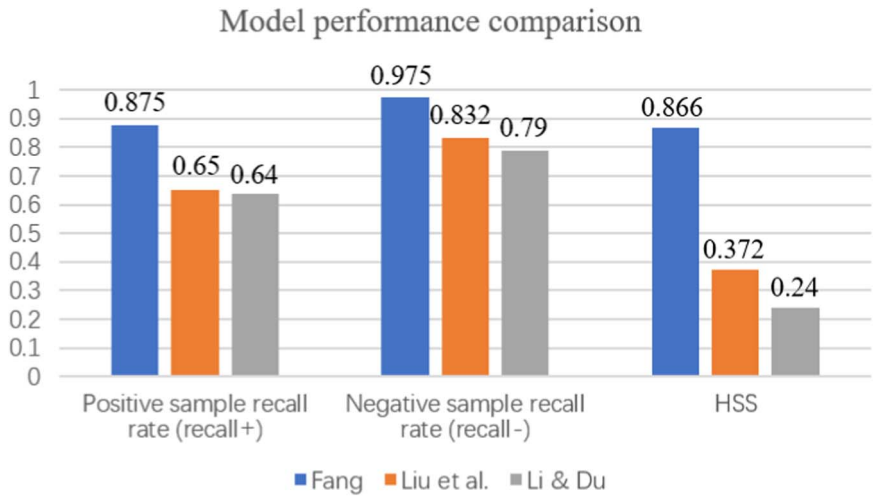

Figure 10. Performance comparison between the fusion model and other methods.

Table 8
Horizontal Comparison of Flare Forecasting Models by Li, Fang, and Wan

	Horizontal Comparison	Whether the Outbreak	ACC	Precision	Recall
Li & Du (2019)	Forecasting model within 30°	N	87.3%	94.2%	88.1%
		P	87.3%	88.2%	71.6%
	Forecasting model beyond 30°	N	68.1%	82.3%	67.5%
		P	68.1%	67.5%	77.2%
Fang (2018)	epoch = 500	N	91.6%	94.8%	92.4%
	batch_size = 8	p	91.6%	85.7%	90.0%
	epoch = 500	N	94.1%	93.9%	97.5%
	batch_size = 16	p	94.1%	94.6%	87.5%
	epoch = 1000	N	90.8%	92.5%	93.7%
	batch_size = 8	p	90.8%	87.2%	85.0%
	epoch = 1000	N	90.8%	93.6%	92.4%
	batch_size = 16	p	90.8%	85.4%	87.5%
Wan et al. (2022)	CNN	N	83.2%	84.6%	82.4%
		p	84.3%	84.8%	83.1%
	GRU	N	86.4%	86.6%	84.5%
		p	87.5%	87.8%	84.9%
	CNN–GRU	N	90.4%	91.2%	89.5%
		p	90.8%	91.4%	90.2%

4.4. Section Summary

The core task of solar flare forecasting is to build a forecast model using statistical ML methods, deep learning methods, or a combination of them, and how to choose a high-performance forecast model is a key problem for experts and scholars to solve. In this section, the single-model and fusion-model design methods, which have been widely used in flare forecasting in recent years, are described. The forecasting performance of these models is analyzed with horizontal comparison, and other forecasting methods are briefly outlined. It is demonstrated that solar flare forecasting models show diversified development, and with regard to statistical ML, a large number of comparative experimental analyses demonstrate that models combining multiple statistical ML methods have better forecasting performance than single-method models. As for deep learning, the sparse connection and weight sharing properties of CNN reduce the total number of parameters in the training process and facilitate CNN to learn flare burst patterns quickly. In addition, RNN and its corresponding variants can better take into account the time-series features of flare data. The fusion model combining these two methods can learn flare outburst patterns more accurately and the quantified metrics of prediction performance are excellent. To further improve the forecast rate, hyperparametric search for the optimization of forecast models, selection of more novel algorithms, and design of models adapting to the imbalance problem of flare observed data are open to further research.

5. Conclusion and Prospection

In summary, we herein review the techniques of solar flare forecasting based on data-driven models in recent years from the aspects of sample feature selection, sample preprocessing, and forecast model design. So far, in the field of solar flare forecasting, most studies use conventional forecast factors, including the sunspots and magnetic field parameters. However, with the advancement of observation techniques, some studies have found that flare outbursts are associated with CMEs (Forbes et al. 2006) and solar energetic particles (SEPs)

(Reames 2013). Therefore, extracting forecast factors from the CME and SEP events can be considered in the future.

Most studies use resampling to deal with the class imbalance problem in flare data, but resampling introduces additional forecast errors. To resolve the problem, it is necessary to consider a range of classifier-based imbalance treatment methods and verify their applicability. Meanwhile, current study mainly deals with inter-class imbalance, whereas intra-class imbalance exists in the flare data, which still needs to be further studied and appropriately addressed.

In terms of ML algorithms, models that combine multiple statistical ML methods have superior forecasting performance compared with single-method models. With regard to deep learning, the fusion model combining CNN and RNN can learn flare outburst patterns more accurately, and the quantified indicators of the forecast performance are much better. To further improve the forecast rate, hyperparameters search for optimization of forecast models, selection of more novel algorithms, and design of models adapting to the imbalance problem are hot topics for future research. In addition, with the development of ML techniques, new algorithms such as recommendation algorithms and self-organizing mapping neural networks (Kholod et al. 2021) have emerged, which can shed new light on flare forecasting.

Acknowledgments

The authors would like to acknowledge the support of the National Key Research and Development Program of China (No. 2022YFA1604600) and the National Natural Science Foundation of China (NSFC, Grant No. 11975086).

ORCID iDs

Jun-feng Fu https://orcid.org/0000-0003-0242-2218

References

Abed, A. K., Qahwaji, R., & Abed, A. 2021, AdSpR, 67, 2544
Anastasiadis, A., Papaioannou, A., & Sandberg, I. 2017, SoPh, 292, 1
Arjun, P., & Manoj, K. G. 2021, CompJ, 2021, 1
Aschwanden, M. J., & Aschwanden, P. D. 2008, ApJ, 674, 530
Batista, G. E., Prati, R. C., & Monard, M. C. 2004, ACM SIGKDD Explorations Newsletter, 6, 20
Beinecke, J., & Heider, D. 2021, BioData Mining, 14, 1
Benvenuto, F., Campi, C., & Massone, A. M. 2020, ApJL, 904, L7
Bertolucci, S., Zioutas, K., & Hofmann, S. 2017, PDU, 17, 13
Bloomfield, D. S., Higgins, P. A., & McAteer, R. T. J. 2012, ApJL, 747, L41
Bobra, M. G., Wright, P. J., & Sun, X. 2021, ApJS, 256, 26
Carrasco, V. M. S., Lefèvre, L., & Vaquero, J. M 2015, SoPh, 290, 1445
Carrington, R. C. 1859, MNRAS, 20, 13
Castelvecchi, D. 2016, Nature News, 538, 20
Chawla, N. V., Bowyer, K. W., & Hall, L. O. 2002, J. Artif. Intell. Res., 16, 321
Chen, J., Li, W., & Li, S. 2022, SpScT, 2022, 452
Chen, Y., Manchester, W. B., & Hero, A. O. 2019, SpWea, 17, 1404
Cicogna, D., Berrilli, F., & Calchetti, D. 2021, ApJ, 915, 38
Cinto, T., Gradvohl, A. L. S., & Coelho, G. P. 2020, SoPh, 295, 93
Colak, T., & Qahwaji, R. 2009, SpWea, 2009, 277
Cui, Y., Li, R., & Zhang, L. 2006, SoPh, 237, 45
Démoulin, P., & Pariat, E. 2008, AdSpR, 43, 1013
Deng, Z., Wang, F., & Deng, H. 2021, ApJ, 922, 232
Deshmukh, V., Berger, T., & Meiss, J. 2020, arXiv:2012.14405
Deshmukh, V., Flyer, N., & Van Der Sande, K. 2022, ApJS, 260, 9
Domijan, K., Bloomfield, D. S., & Pitié, F. 2019, SoPh, 294, 1
Doschek, G. 2021, SoPh, 296, 1
Edmonds, I. R. 2018, arXiv:1811.10703
Falco, M., Costa, P., & Romano, P. 2019, JSWSC, 9, 22
Fang, R. 2018, Beijing University of Posts and Telecommunications, (In Chinese), https://kns.cnki.net/KCMS/detail/detail.aspx?dbname=CMFD201802&filename=1018096349.nh
Florios, K., Kontogiannis, I., & Park, S. H. 2018, SoPh, 293, 1
Forbes, T. G., Linker, J. A., & Chen, J. 2006, Coronal Mass Ejections, 2006, 251
Fu, X., Liao, C. W., & Bai, X. Y. 2018, AR&T, 15, 340, (In Chinese)
Gallagher, P. T., Moon, Y. J., & Wang, H. 2002, SoPh, 209, 171
Gopalswamy, N., Lara, A., & Yashiro, S. 2003, ApJL, 598, L63
Guerra, J. A., Pulkkinen, A., & Uritsky, V. M. 2016, SpWea, 13, 626
Gyenge, N., Ludmány, A., & Baranyi, T. 2016, ApJ, 818, 127
Hale, G. E. 1908, Terr. Magn. Atmos. Elect., 13, 59
Han, H., Wang, W. Y., & Mao, B. H. 2005, in International Conference on Intelligent Computing, ed. D. S. Huang, X. P. Zhang, & G. B. Huang, 677
Hazra, S., Sardar, G., & Chowdhury, P. 2020, A&A, 639, A44
He, H., & Garcia, E. A. 2009, IEEE Trans. Knowl. Data Eng., 21, 1263
He, X. R. 2021, CNKI, 2021 (In Chinese), 23
Higgins, P. A., Gallagher, P. T., & Mcateer, R. 2011, AdSpR, 47, 2105
Huang, G., Liu, Z., & Laurens, V. 2016, IEEE Computer Society, 234, 4700
Huang, X., Wang, H., & Xu, L. 2018, ApJ, 856, 7
Huang, X., Yu, D., & Hu, Q. 2010, SoPh, 263, 175
Hunter, D. A., Gallardo, S., & Zhang, H. X. 2018, ApJ, 855, 7
Inoue, S., Bamba, Y., & Kusano, K. 2017, JASTP, 180, 3
Jonas, E., Bobra, M., & Shankar, V. 2018, SoPh, 293, 1
Khan, R. U., Zhang, X., & Kumar, R. 2019, JCVHT, 15, 29
Kholod, I., Rukavitsyn, A., & Paznikov, A. 2021, J. Supercomputing, 77, 6197
Komm, R., & Hill, F. 2009, JGRA, 114, 78
Korsós, M. B., Ludmany, A., & Erdelyi, R. 2015, ApJL, 802, L21
Korsós, M. B., Romano, P., & Morgan, H. 2020, ApJL, 897, L23
Korsós, M. B., Ruderman, M. S., & Erdélyi, R. 2018, AdSpR, 61, 595
Krista, L. D., & Chih, M. 2021, ApJ, 922, 218
Kusano, K., Iju, T., & Bamba, Y. 2020, Science, 369, 587
Landa, V., & Reuveni, Y. 2022, ApJS, 258, 12
Li, R., & Du, Y. 2019, AdAst, 2019, 1
Li, R., & Huang, X. 2018, SSPMA, 48, 119601
Li, R., Wang, H., & Cui, Y. M. 2011, SCPMA, 54, 1546
Lim, D., Moon, Y. J., Park, J., et al. 2019, JKAS, 52, 133
Liu, C., Deng, N., & Wang, J. T. L. 2017a, ApJ, 843, 104
Liu, H., Liu, C., & Wang, J. 2019, ApJ, 877, 121
Liu, J. F., Li, F., & Wan, J. 2017b, RAA, 17, 34
Liu, J. F., Li, F., & Zhang, H. P. 2017c, RAA, 17, 116
Louis, R. E., Kliem, B., & Ravindra, B. 2015, SoPh, 290, 3641
Lu, S., Lu, Z., & Zhang, Y. D. 2018, JComS, 30, 41
Ma, J., Liu, Z., & Shi, Y. R. 2021, Spacecraft Environment Engineering, 38, 256, (In Chinese)
Ma, R., Boubrahimi, S. F., & Hamdi, S. M. 2017, in IEEE International Conference on Big Data (Big Data) 2017, ed. M. Khalefa, S. D. Bhattacharjee, & D. J. Crichton, 2569
McIntosh, P. S. 1990, SoPh, 125, 251
Morales, L., & Charbonneau, P. 2016, ApJ, 682, 654
Murray, S. A., Bingham, S., & Sharpe, M. 2017, SpWea, 15, 577
Nandy, D. 2020, SoPhys, 296, 3
Ndacyayisenga, T., Uwamahoro, J., & Raja, K. S. 2021, AdSpR, 67, 1425
Nishizuka, N., Sugiura, K., & Kubo, Y. 2017, ApJ, 835, 156
Nishizuka, N., Sugiura, K., & Kubo, Y. 2018, ApJ, 858, 113
Niu, Z., Zhong, G., & Yu, H. 2021, Neurocomputing, 452, 48
Nurzaman, M. Z., & Dani, T. 2019, JPhCS, 1231, 012020
Osokin, A. R., Podlazov, A. V., & Chernetsky, V. A. 2004, Proc. Int. Astron. Union, 2004, 477
Panos, B., & Kleint, L. 2020, ApJ, 891, 17
Park, E., Moon, Y. J., & Shin, S. 2018, ApJ, 869, 91

Park, J., Moon, Y. J., & Choi, S. 2017, SpWea, 15, 704
Park, S. H., Leka, K. D., & Kusano, K. 2020, ApJ, 890, 124
Petrakou, E. 2021, AdSpR, 68, 2963
Ramraj, S., Uzir, N., & Sunil, R. 2016, IJCTA, 9, 276
Reames, D. V. 2013, SSRv, 175, 53
Ribeiro, F., & Gradvohl, A. L. S. 2021, A&C, 35, 100468
Rong, L., Jie, Z., & YanMei, C. 2013, ChSBu, 58, 1845
Roy, S., Prasad, A., & Ghosh, K. 2020, RAA, 20, 110
Sadykov, V. M., & Kosovichev, A. G. 2017, ApJ, 849, 148
Sharma, J., Kumar, B., & Malik, A. K. 2021, MNRAS, 506, 4952
Shibata, K., & Magara, T. 2011, Living Rev. SoPh, 8, 6
Shin, S., Lee, J. Y., & Moon, Y. J. 2016, SoPh, 291, 897
Stanislavsky, A., Burnecki, K., & Janczura, J. 2019, MNRAS, 485, 3970
Stanislavsky, A., Nitka, W., & Małek, M. 2020, JASTP, 208, 105407
Su, Y., Dong, L., & Niu, Y. 2019, Prog. Geophys., 34, 1336
Sun, J., & Li, H. 2008, Expert Syst. Appl., 35, 818
Sun, Z., Bobra, M. G., & Wang, X. 2022, ApJ, 931, 163
Suykens, J. A. K., Van, Gestel, T., & De, Brabanter, J. 2002, Basic Methods of Least Squares Support Vector Machines, 10 (Singapore: World Scientific), 71
Tang, R., Liao, W., & Chen, Z. 2021, ApJS, 257, 50
Tao, X., Li, Q., & Guo, W. 2019, Inf. Sci., 487, 31
Vemareddy, P., Ambastha, A., & Maurya, R. A. 2012, ApJ, 761, 86
Vemareddy, P., Cheng, X., & Ravindra, B. 2016, ApJ, 829, 24
Vuttipittayamongkol, P., & Elyan, E. 2020, Inf. Sci., 509, 47
Wan, J., Fu, J. F., & Tan, D. M. 2022, RAA, 22, 085020
Wang, J., & Duan, B. 2017, CAAI Transactions on Intelligent Systems, 12, 865, (In Chinese)
Wang, X., Wu, J., & Liu, C. 2017, J. Beijing Univ. Aeronaut. Astronaut., 44, 772
Wang, Z., Wu, C., & Zheng, K. 2019, IEEE Access, PP, 1
Wheatland, M. S. 2004, PASA, 22, 153
Yi, K., Moon, Y. J., & Lim, D. 2021, ApJ, 910, 8
Yi, K., Moon, Y. J., & Shin, G. 2020, ApJL, 890, L5
Yu, D., Huang, X., & Wang, H. 2009, SoPh, 255, 91
Yu, L., Zhou, R., & Tang, L. 2018, Appl. Soft Comput., 69, 192
Yuan, F., Lin, J. B., & Deng, Y. Y. 2016, ChSBu, 61, 2316, (In Chinese)
Zheng, Y., Li, X., & Wang, X. 2019, ApJ, 885, 73
Zhou, Y., Lin, Q., & Xiao, D. 2002, JPhCS, 2294, 012035